Switched Parasitic Elements for Antenna Diversity

Rodney Vaughan, *Senior Member, IEEE*

***Abstract*—Switched parasitic elements provide a useful implementation of antenna pattern diversity. The basic principle is presented with some examples of wire antennas computed using the method of moments. The modeled diversity gain available from selection combining of uncorrelated signals is used to quantify the expected improvement relative to nondiversity antennas. The advantage of the switched parasitic concept is that it is a relatively simple system, which can give the adaptive antenna performance of many branch selection or switched diversity.**

***Index Terms*— Antenna arrays, antenna radiation patterns, diversity, mobile communications, multibeam antennas, personal communications.**

I. Introduction

In mobile and personal radio communications, multipath propagation degrades the communication link. In dense multipath, the antenna directivity is considered to be in a distributed direction and the antenna gain can be treated as a statistical quantity called the effective gain. The narrowband channel features signal fading in which the fades can be as close as a half wavelength, and whose envelopes are Rayleigh distributed. The Rayleigh fading limits the capacity of the link. A method for mitigating the effect of the fading is to use antenna diversity.

This paper presents a class of simple antennas that produce diversity action and offer performance improvement over conventional single-port (nondiversity) antennas. The antenna system comprises an "active" element, which is permanently connected to the receiver, and parasitic elements, which have strong mutual coupling with the active element. The parasitic elements have a switchable terminating impedance. The different switch settings result in different far-field patterns and these patterns invoke different fading in the channel of the active element. The advantage of the system is that it is a simpler configuration than that of conventional antenna diversity where receivers or signal multiplexers are connected to each element. Finding the element configurations is the antenna design problem here. It requires a knowledge of or a statistical model for the multipath propagation which provides the incident power at the antenna. A statistical model is used, which is uniform in the azimuth coordinate in the direction of the horizon [1]. The antenna configurations used here often feature rotational symmetry in the available far-field patterns and so the mechanism for the diversity action is often "angle diversity."

Manuscript received February 4, 1996; revised July 30, 1998. This paper was supported in part by the Center for PersonKommunikation, Aalborg University, Denmark.

The author is with the New Zealand Institute of Industrial Research Limited, Lower Hutt, New Zealand.

Publisher Item Identifier S 0018-926X(99)02477-1.

II. Patterns for Antenna Diversity

The basic principle of antenna diversity is to have patterns that are orthogonal, or at least reasonably uncorrelated, over the incident multipath field distribution. The switched parasite concept allows the signals from different patterns to be received at the same antenna port with the obvious constraint that only one pattern can be used at a time. This contrasts with the usual multiple-port diversity antennas whose signals are available at different ports simultaneously [2], [3].

For diversity patterns, we consider two far-field patterns E_1 and E_2, which are normalized in the sense

$$\int_0^{2\pi}\int_0^{\pi} S(\theta,\,\phi)|E_1(\theta,\,\phi)|^2 \sin\theta\, d\theta\, d\phi = 1 \qquad (1)$$

(and similarly for E_2), where $S(\theta,\,\phi)$ is the probability density function (pdf) of incident waves referred to the antenna coordinates and is called the *scenario*. Under certain assumptions the correlation coefficient of the zero-mean signal voltages received by the two patterns is [4]

$$\rho_{12} = \int_0^{2\pi}\int_0^{\pi} S(\theta,\,\phi)E_1(\theta,\,\phi)\cdot E_2^*(\theta,\,\phi)\sin\theta\, d\theta\, d\phi. \qquad (2)$$

Ideally, the correlation coefficient should be zero for Rayleigh fading envelopes, but it is well known [2], [3] that effective diversity action can be obtained as long as the envelope correlation coefficient $\rho_{e12} \approx |\rho_{12}|^2$ is less than about 0.7. The basic design (2) reduces for simplistic, but reasonable, modeled scenarios. Further details can be found in [3] and [4].

The Clarke scenario [1] has a pdf $1/(2\pi \sin\theta)\delta(\theta-\pi/2)$. The correlation coefficient now becomes

$$\rho_{12} = \frac{1}{2\pi}\int_0^{2\pi} E_1(\phi)E_2^*(\phi)\, d\phi \qquad (3)$$

where $E_1(\phi) = E_1(\theta = \pi/2,\,\phi)$ in the chosen polarization, and similarly for E_2; and ϕ is the usual azimuthal angle. Patterns with low ρ_{12} are sought. In the following section, a correlation coefficient function

$$\rho_{11}(\gamma) = \frac{1}{2\pi}\int_0^{2\pi} E_1(\phi)E_1^*(\phi+\gamma)\, d\phi \qquad (4)$$

is used as an estimate for the ρ_{12} for signals from rotated (by an angle γ) antenna configurations (see below). The envelope correlation coefficient of the signals received from the beams is taken as $\rho_{e11} \approx |\rho_{11}|^2$, and similarly for ρ_{e12}.

Under the assumption of continuous, uncorrelated, constant density scatterers comprising the two-dimensional (2-D) scenario, the mean 2-D directivity to the scatterers is independent of the pattern shape. This can be explained as follows. As a pattern becomes more directive, a decreasing quantity of

scatterers illuminate the receiving pattern with increasing power gain to the receiver, resulting in the received power remaining constant. (It is assumed for now that the antenna efficiency and matching is independent of the directivity in order to relate the directivity to the average received power.)

The scenario is defined or rather it is postulated as a model from a time-averaged (i.e., position-averaged for a mobile terminal) distribution of scatterers. In practice, the *instantaneous* distribution of scatterers changes with time and position and so a more directive beam will provide greater fluctuations in the received power as strong scatterers move in and out of the directive beam. However, under the assumptions of the scenario model, the time-averaged power entering the beam will be the same. In summary, the mean and variance of the received power are independent of the antenna directivity for uniform, distributed models such as the Clarke scenario; but in practice, the variance of the received power may increase with increasing directivity although the true (long term) mean of the received power should remain the same, i.e., independent of the directivity.

The diversity performance is generally measured as *diversity gain*, which is also a time-averaged quantity. For an increasing correlation coefficient, the diversity gain decreases, but this dependence is weak as long as the correlation coefficient is small [2], [3]. The diversity gain also decreases as the difference in the mean gains of the diversity branches of the diversity antenna increases [2]–[5].

The diversity gain is the ratio of the (best) single branch signal-to-noise ratio, γ_1, relative to its mean value over the fading, Γ_1, i.e., (γ_1/Γ_1); and the combined-signal-to-combined-noise ratio relative to its mean value, i.e., (γ_c/Γ_c), for a given signal level probability. The diversity gain is thus the improvement in signal-to-noise ratio for a given "outage time." It can be written in decibels as

$$DG\,(\mathrm{dB}) = \left[\frac{\gamma_c}{\Gamma_c}\,(\mathrm{dB}) - \frac{\gamma_1}{\Gamma_1}\,(\mathrm{dB})\right]_{\text{Probability given}} \tag{5}$$

and the ratios within this equation are found from the signal cumulative probability functions. For switched combining of two uncorrelated Rayleigh distributed envelopes, the maximum diversity gain for an outage of 1% is about 10 dB (corresponding to a switching threshold of about 10 dB below the mean signal level). For selection combining, an outage of 1% corresponds to about 10 dB (2 branches), 15 dB (4), and 17 dB (6) at which diminishing returns for increasing branch numbers have set in. These values represent the highest possible diversity gains from the antenna types discussed in this paper, however, the diversity gain increases as the outage criteria tightens.

III. Switched Parasite Antennas

Adams and Warren [6] and Zhang *et al.* [7] have analyzed the short-circuit and open-circuit cases numerically using the moment method. However, the use of switched parasites for controlling patterns goes back to the work of Yagi and Uda during the 1930's and has been patented in various forms for various applications, for example, by Gueguen [8] and many others too numerous to mention. In mobile communications, Milne [e.g., 9] has used this concept for multiple switched elements for a vehicular satellite (point-to-point) communications antenna, and Hamer and Butcher [10] have simulated a single-switched element design for vehicular use and also investigated impedance. Here, the interest is confined to simple configurations in order to demonstrate some of the possibilities in mobile and personal communications. A general treatment of impedance is not attempted here, but results from the particular moment method, which uses delta-gap excitation, are given for reference.

With a single-switched element, the impedance of the active element varies with the switch state of the parasite. The closer the parasite, the more the pattern and the impedance changes, since the mutual coupling is greater. For compact designs [cf. Fig. 1(a)] where the spacing is small, the large change in the impedance becomes a problem. A solution is to introduce another element switched in opposition to the first so that the active element "sees" a similar configuration (i.e., rotationally symmetric or mirror image) for each switch setting. Examples are suggested in Fig. 1(b) and (c). In Fig. 1(c), the arrangement could be two short-circuit elements and one open-circuit element. This can be vice versa (i.e., two opens and one short) in which case the active element will "see" a different arrangement and have a different input impedance. Fig. 1(d) shows a conceptual implementation of the 1(b) antenna configuration applied to a handheld terminal. For three parasites, there are three different patterns (same pattern rotated) for both arrangements (mirror images). For many element designs, the symmetry requirement can be relaxed, depending on constraints on the impedance change. The number of available patterns increases quickly with the number of parasitic elements.

Finally, a note to clarify the antenna coupling is in order. The input impedance to the "active" element (denoted 1) can be expressed as

$$Z_1^{(\mathrm{IN})} = Z_{11} + Z_{12}\left(\frac{I_2}{I_1}\right) + Z_{13}\left(\frac{I_3}{I_2}\right) + \cdots \tag{6}$$

where 2 and 3, $\cdots$ denote the respective parasitic elements, and the currents entering the elements are $I_1, I_2, I_3, \cdots$. The mutual impedances between elements, e.g., Z_{12}, are defined from the antenna geometry, i.e., they are independent of terminating impedances. The switched terminations on the parasites create a change in the currents and a corresponding change in the input impedance. In accepted terminology, the *mutual coupling* is the complicated interaction of the close elements and the *mutual impedance* is a fixed parameter of the antenna.

IV. Examples

A. Example 1: Two Patterns from a Compact Antenna

On a hand-held terminal, it is necessary to have compact antennas, which is increasingly viable with the increasing frequencies used for personal communications. For example, eight effectively decorrelated antennas have been demonstrated

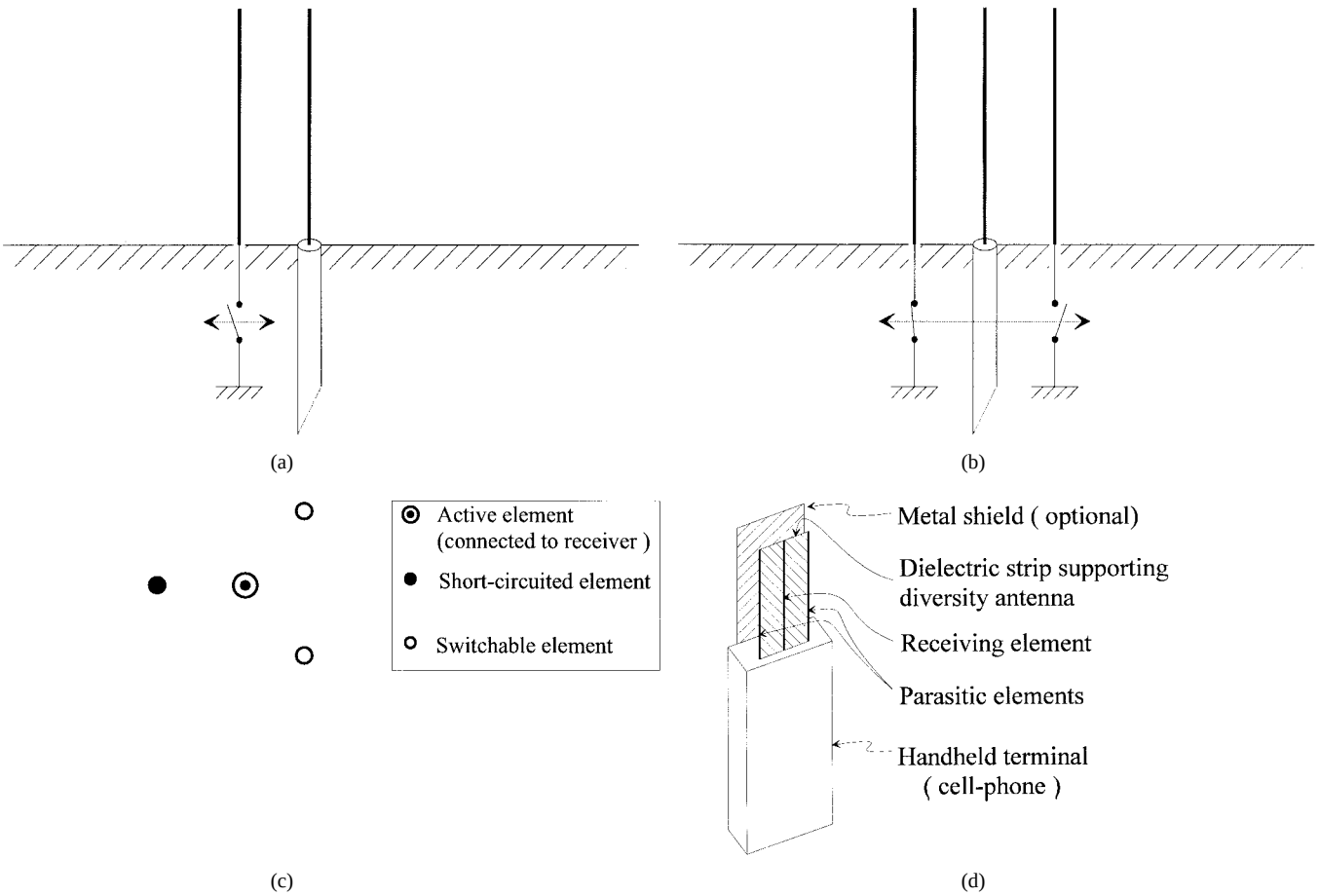

Fig. 1. (a) The basic configuration for a switched parasitic element close to the receiving element. The impedance of the receiving element is affected by the state of the termination of the parasite. (b) A symmetric configuration that allows a stable impedance for the receiving element by switching the parasites in opposition. (c) Plan view of a three-parasitic element configuration. The switching of the elements is coordinated to maintain the impedance of the receiving element. (d) One possible implementation of the antenna of Fig. 1(b) for a handheld terminal.

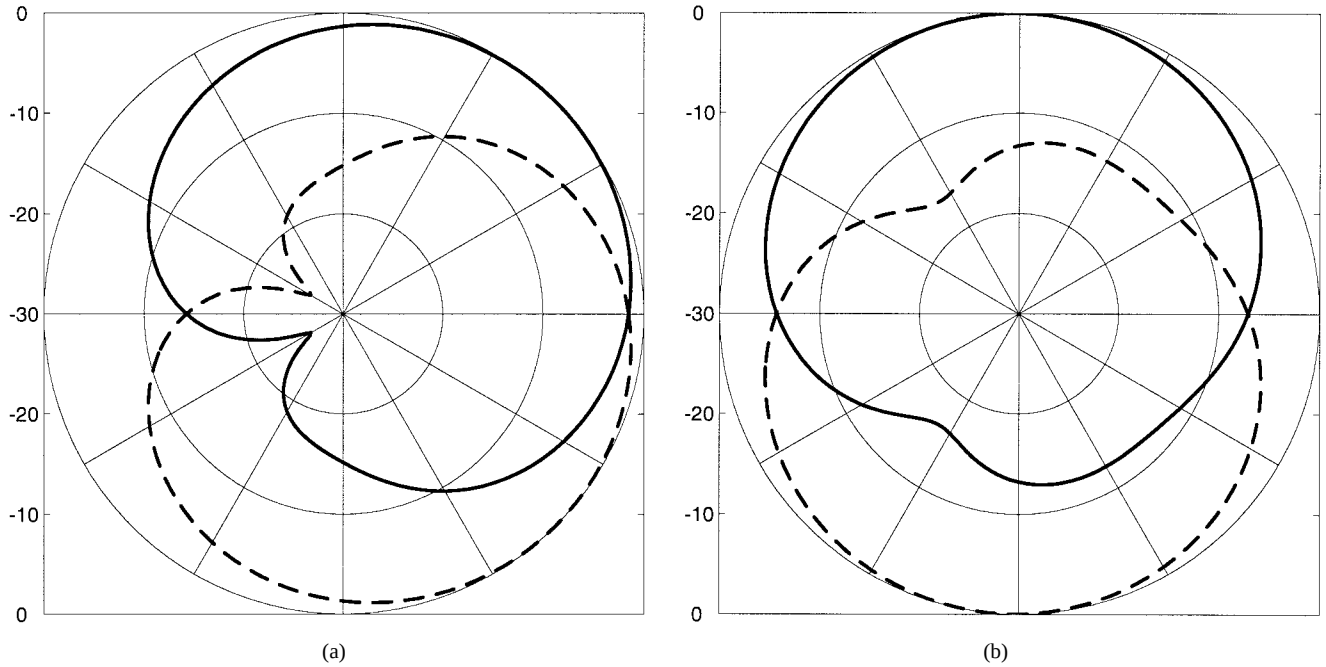

Fig. 2. (a) Far-field power patterns for the configurations of Fig. 1(c) with the interelement distance $d = 0.1\lambda$. (b) For $d = 0.05\lambda$. Scales are 30 dB with 10 dB between rings.

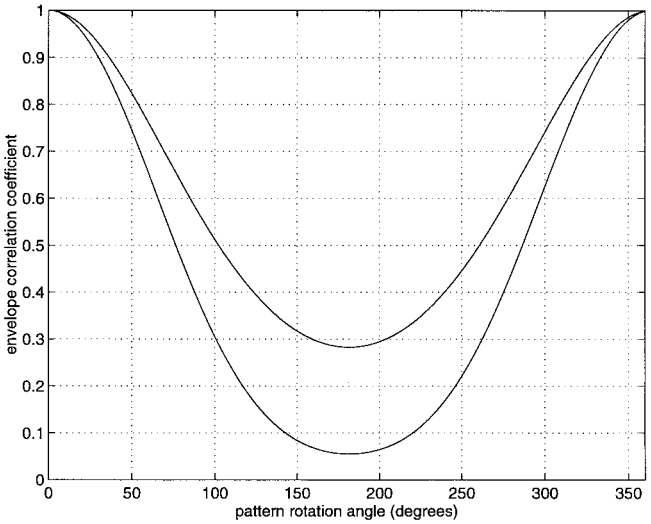

Fig. 3. The envelope correlation coefficient of signals received by the pattern of Fig. 2(a), as the pattern is rotationally spaced in a homogeneous distributed source scenario. The upper trace is for the pattern as a real function and the lower trace is for the complex pattern.

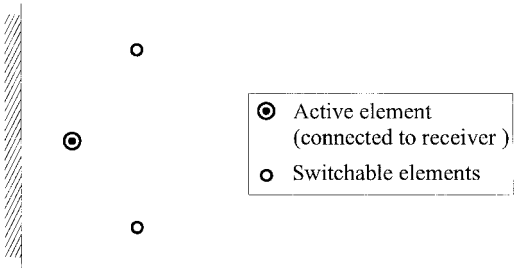

Fig. 4. The configuration where the permanently short-circuited element in Fig. 1(c) is replaced by an infinite ground plane.

on a hand held for 1.5 GHz [11]. It is also desirable to direct the pattern away from the head to maintain radiation efficiency [12], [13]. The arrangement in Fig. 1(c), with the indicated short-circuited element fixed, gives two patterns with some directionality which can be deployed to be away from the head. The element closest to the head is a fixed (short-circuited) reflector and the other two elements are directors. MININEC II code was used to produce the patterns which were computed for a distance of 15λ from the antenna. The numerical implementation was monopoles on an infinite ground plane with all elements having ten pulse functions and a wire radius of 0.0005λ.

In the example, the reflector is 0.27λ long, the "active" (receiving) element is 0.25λ, the directors are 0.23λ and the interelement spacing is $d = 0.1\lambda$. The open circuit was created by raising the element by 0.01λ above the ground plane. The impedance of the active element is $13 - j31\Omega$. The correlation coefficient for the signals received from a homogeneous scenario is $0.62 + j0$ giving an envelope correlation coefficient of $\rho_e \sim |\rho_{12}|^2 \sim 0.38$. For an interelement spacing of $d = 0.05\lambda$, the impedance is $1.4 - j23\Omega$; the correlation coefficient is $\rho_{12} = 0.24 - j0$, so the envelope coefficient is essentially zero from $\rho_e \approx |0.24 - j0|^2 \approx 0$. The pattern for this configuration is given in Fig. 2(b). The pattern is not so directive as that with $d = 0.1\lambda$.

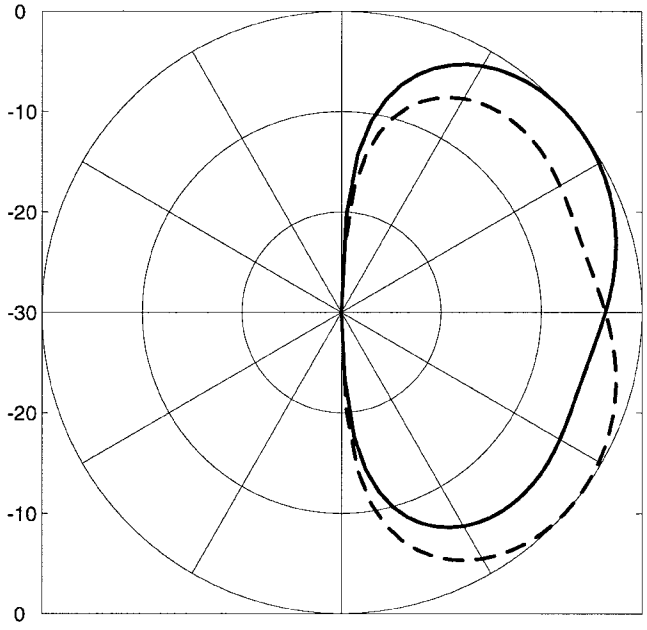

Fig. 5. The far-field power patterns for the patterns from the configurations of Fig. 4.

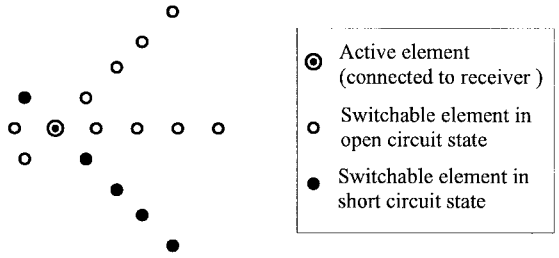

Fig. 6. A configuration for a three Yagi–Uda antennas, which can be selected by switched elements.

By rotating the pattern of Fig. 2(a), the envelope correlation function of the fading signals from the two patterns in the Clarke scenario can be found using (4). The function is given in Fig. 3 for the cases where the patterns are treated as complex as well as purely real. For the real pattern case, only the pattern magnitude is considered by using the substitution $E_1(\phi) \longleftarrow |E_1(\phi)|$ in (4). This is called the real pattern from now on. Comparing correlation functions from real patterns and complex patterns reveals the effect of the phase of the patterns on the decorrelation. In this example, the effect of the phase is considerable, decreasing the $\rho_e = 0.7$ correlation angle from about 64 to 53°. The corresponding curves for the $d = 0.05\lambda$ configuration are closer together and fall in between the two $d = 0.1\lambda$ curves presented. This closeness of the curves suggests that the different amplitude functions of the patterns is the dominant decorrelation mechanism, i.e., "angle diversity." The value of 53° indicates that some 360/53 ≈ 6–7 angularly spaced patterns (i.e., six to seven parasitic elements at the 0.1λ spacing from the active element) from this antenna arrangement (i.e., two elements shorted, angularly spaced by 120°) are available for providing mutually uncorrelated diversity branches.

The limit to compactness is similar to that in superdirective arrays—high currents and strong reactive fields ultimately render the antenna arbitrarily compact but hopelessly inefficient.

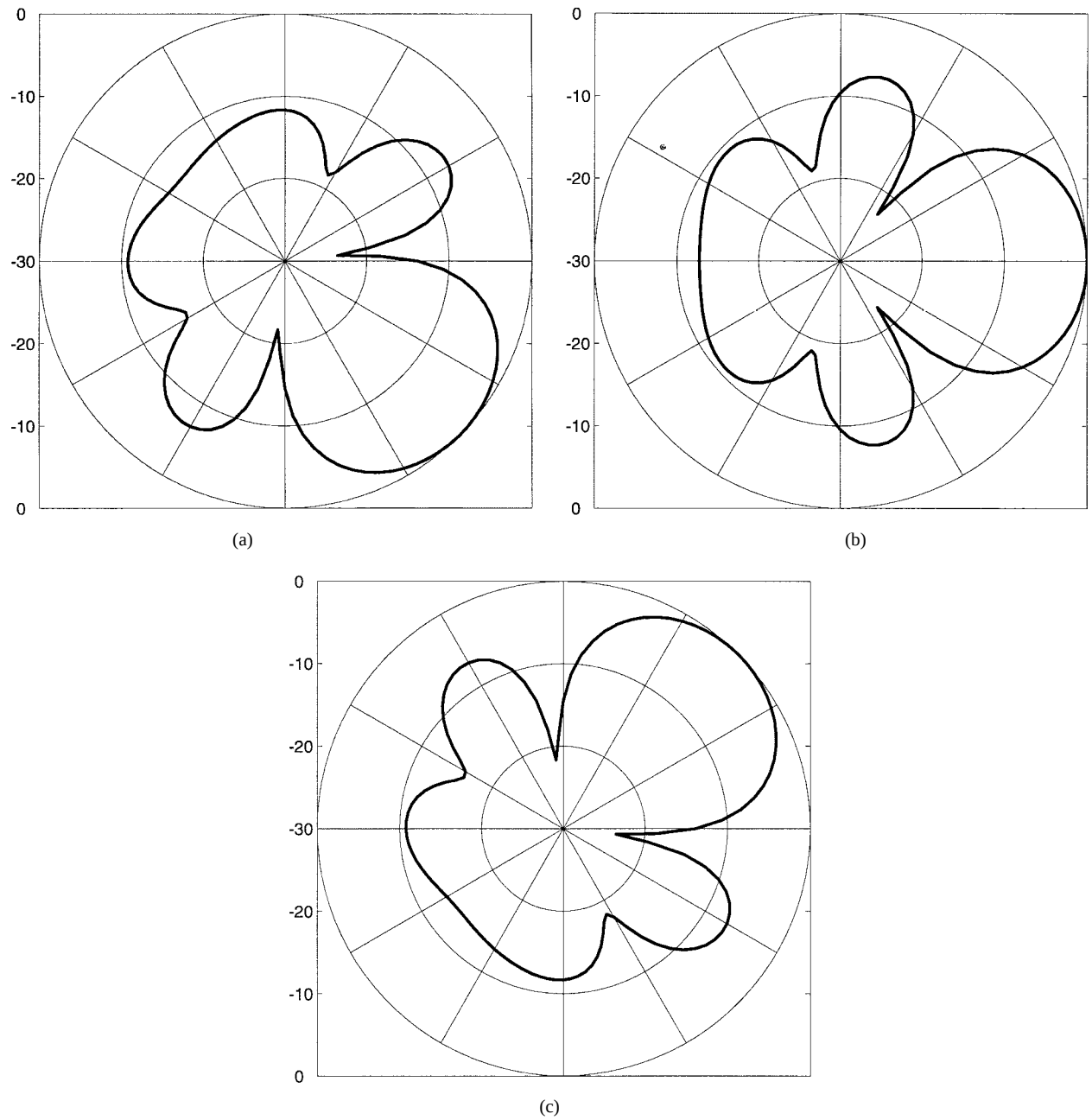

Fig. 7. The far-field power patterns for the Yagi antennas. The full scale is 30 dB with 5 dB between rings. The 45° pattern is nearly identical to the 0° pattern.

B. Example 2: Two Patterns in Half-Space

The same example as above is used, but where one of the short-circuited parasitic elements of Fig. 1(c) is replaced by a ground plane, as depicted in Fig. 4. The two available power patterns (resulting from different switch settings) are given in Fig. 5. For a homogeneous uncorrelated source distribution over the half-space, the envelope correlation coefficient is $\rho_e \approx |-0.06 + j0|^2 \approx 0$. For the real pattern case, this changes to $\rho_e \approx |0.91 + j0|^2 \approx 0.83$. Comparing these two results indicates that the phase of the pattern is dominant as the decorrelation mechanism in the Clarke scenario. By considering the images of the elements in the ground plane, the large difference between, and the relative complexity of, the element configurations is seen as the reason for producing such phase dominance.

This example and the previous example provide limiting cases for when the fixed reflector element is a finite plate. An infinitesimally narrow plate is like a thin wire and a very wide plate is like an infinite "ground plane" for the hemisphere of interest. A finite plate can fit onto a hand held [11] or be part of a wall-mounted base-station antenna.

C. Example 3: Multiple Uda–Yagi

The configuration for three possible Uda–Yagi antennas of Fig. 6 is computed. The separation between the elements of each Uda–Yagi is 0.2λ. The example uses six elements for each beam and the element sets have an angular separation of 45°. The patterns, shown in Fig. 7, are essentially unaffected by the open-circuit elements, as expected. The half-power beamwidth (HPBW) is about 52°. The open circuits in this example

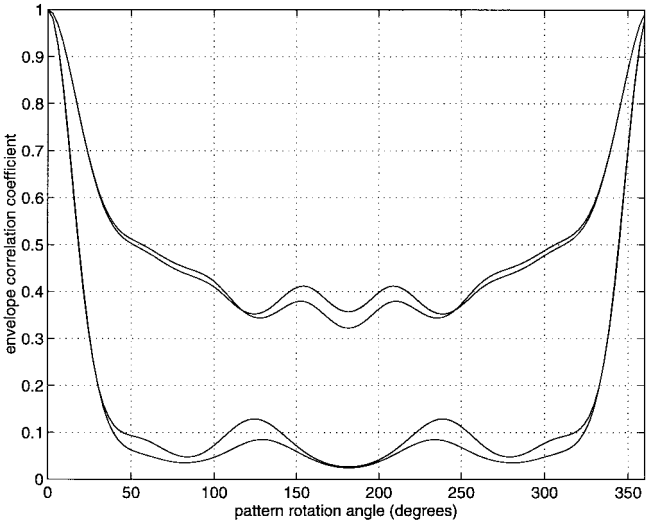

Fig. 8. The envelope correlation function for the two slightly different Yagi patterns. The upper pair are the patterns as real functions and the lower pair are for the complex patterns.

comprise 10 kΩ resistances at the bases of the switchable element. This gives very similar results to modeling the open circuits by raising the elements just above the ground plane for including a small air gap. The computed impedances are $31.5 + j13.9\Omega$ for the central beam and $28 + j13\Omega$ for the outer beams.

The $-45°$ beam is denoted a, the $0°$ beam is denoted b, and the $+45°$ beam is denoted c. For homogeneous incident fields, the envelope correlation coefficient $\rho_{eab} = \rho_{ebc} \approx |0.25 + j0.01|^2 \approx 0.06$; and $\rho_{eac} \approx |-0.05 + +j0|^2 \approx 0$. More beams and/or greater directivity could be included with more parasitic elements.

The decorrelation of the beams by rotation is given as a function of rotation angle in Fig. 8. This figure is computed using the patterns calculated from the above Yagi designs, again using (3). However, the result is similar to a cross correlation between realizable patterns (2) since the pattern shape does not change appreciably with the presence of the open-circuited elements in a second antenna. The similarity is intimated in the figure, where the pairs of closer traces are the functions for the central and outer beams. The larger separation of the traces in the figure is for the real and complex beams. For an envelope correlation of 0.7, the angular spacing for this Uda–Yagi antenna pattern in a homogeneous distributed scenario is about 13°. The phase has a large impact on the $\rho_e = 0.7$ beam correlation angle, which goes from about the 13° for the complex pattern, to about 23° for the real pattern, which corresponds to the beams overlapping at the -0.6 and -2.3 dB levels, respectively. The minimum angular spacing required for signal decorrelation using this antenna is thus about 13° and this gives a guideline for the implementation of an antenna.

D. Example 4: Lower Directivity Beam with Fine Rotational Control

The 16-parasitic element configuration of Fig. 9 has a radial distance to the parasites of 0.25λ. This gives the

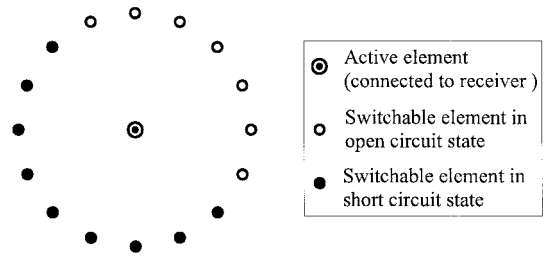

Fig. 9. A 16-element circular configuration in which seven elements are short circuited. The beam can be steered around in 22.5° steps. The radius for the example here is 0.25λ.

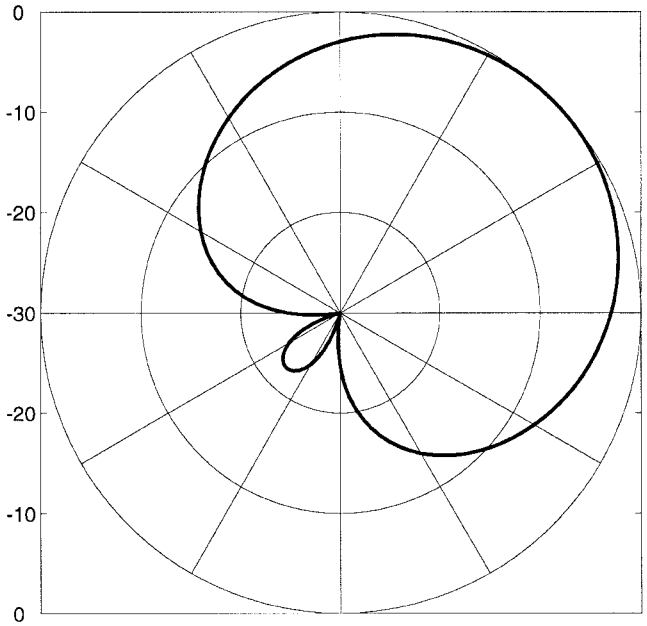

Fig. 10. The far-field power pattern for the 16-element configuration. The full scale is 30 dB.

power pattern in Fig. 10. The HPBW is about 90° and the impedance is about $21 - j6\Omega$. The pattern can be rotated by angles of $360/16 = 22.5°$ by switching the parasites. The choice of having 16 elements is arbitrary; the object of having many elements is that the arrangement gives the possibility of gradient-type algorithms that use the gentle transitions between adjacent patterns. This can act to decrease the bit errors resulting from abrupt phase transitions in the received signal caused by abrupt pattern changes in a few-element antenna. Adjacent patterns (spacing of 22.5°) in this example have an envelope correlation coefficient of about 0.91, which can mean relatively small disturbances to the received modulated signal while switching between patterns. A very large number of decorrelated patterns can be obtained through such a many-element antenna concept. The symmetry requirement can be relaxed in this larger antenna, as mentioned above, since the impedance is rather insensitive to changes in a few elements out of 16 and which, additionally, are well spaced from the active element. The rotational decorrelation angle (from Fig. 11) for homogeneous scenarios is 45 and 50° (again, for an envelope correlation coefficient of 0.7) for the complex and real patterns, respectively. This closeness

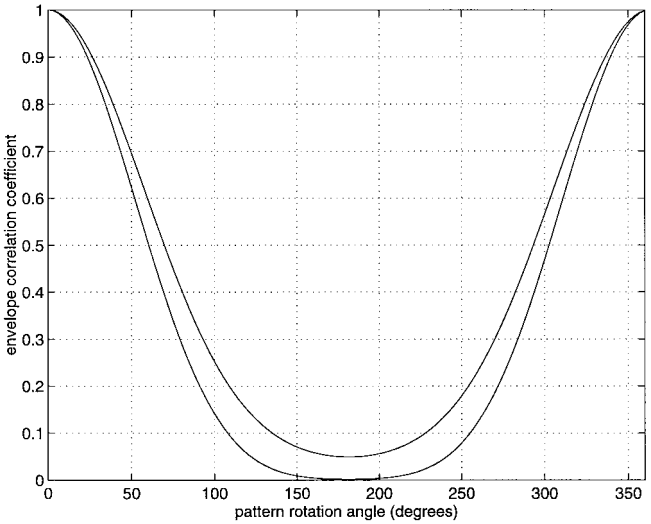

Fig. 11. The envelope correlation function for the rotated pattern of the 16-element configuration. The upper trace is for the pattern as a real function, and the lower trace is for the complex pattern.

indicates that the amplitude of the pattern is the dominant decorrelation mechanism. However, decorrelation need not be via the directionality; the phase degree of freedom is effective when different sets (nonadjacent) elements are short circuited. Reasonably omnidirectional patterns can be obtained from the basic element configuration, which are decorrelated by the phase difference of the patterns (cf. space diversity, where the amplitude patterns are identical and the phase difference between the patterns is the electrical distance of the antenna spacing).

No attempt was made to match the active element in the examples above. The length of the receiving element can be adjusted to tune out reactance, and the length of the parasitic elements influences the resistance.

Finally, it should be noted that in using the patterns to derive the diversity performance, the effect of the very close environment, such as the antenna mounting, is not accounted for here. The ideal situation of isolated dipoles (monopoles on an infinite groundplane), for example, has different patterns to those of monopoles (or sleeved monopoles, etc.) on a hand-held case and in the presence of a head. However, in starting with patterns which are generically promising, the experience has been that the effect of the case and head does not significantly correlate the signals for cases where diversity is required.

V. Conclusion

The design concept and formulation for deriving diversity antenna patterns can be applied to switched parasitic element implementations. Examples have been given that can be used for handheld terminals, vehicular rooftop mounting, and base-station requirements. Advantages of the approach are that retrofits to existing antennas may be possible, there is no switching in the direct RF signal path (although, strictly speaking, the switched elements comprise RF paths), and the design for different pattern requirements is straightforward. The approach could also be applied to other antenna types, for example, switched shorting pins in patch antennas, e.g., [14] and the short circuiting of parasitic slots. Finally, the technique could also be applied to arrays of active elements, where the element pattern can be changed. Such application is thus restricted to small-beam alterations, but subtle beamforming also has applications in personal communications [cf. 15]. A disadvantage for very compact implementations is that matching is normally required.

References

[1] R. H. Clarke, "A statistical theory of mobile radio reception," *Bell Syst. Tech. J.*, vol. 47, pp. 957–1000, 1969.
[2] J. N. Pierce and S. Stein, "Multiple diversity with nonindependent fading," *Proc. IRE*, vol. 48, pp. 89–104, Jan. 1960.
[3] W. C. Jakes, Ed., *Microwave Mobile Communications.* New York: Wiley, 1974 (reprint New York: IEEE Press, 1993).
[4] R. G. Vaughan and J. Bach Andersen, "Antenna diversity in mobile communications," *IEEE Trans. Veh. Technol.*, vol. VT-36, pp. 149–172, Nov. 1987.
[5] Y. Ebine and Y. Yamada, "Vehicle-mounted diversity antennas for land mobile radios," in *Proc. IEEE Conf. Veh. Technol.*, Philadelphia, PA, June 1988, pp. 326–333.
[6] A. T. Adams, "Dipole plus parasitic element," *IEEE Trans. Antennas Propagat.*, vol. AP-19, pp. 536–537, July 1971.
[7] Y. Zhang, K. Hirasawa, and K. Fujimoto, "Opened parasitic elements nearby a driven dipole," *IEEE Trans. Antennas Propagat.* vol. AP-34, pp. 711–713, May 1986.
[8] M. Gueguen, "Electronically step-by-step rotated directive radiation beam antenna," U.S. Patent 3 846 799, filed Aug. 1973, issued Nov. 1974.
[9] R. M. T. Milne, "A small adaptive array antenna for mobile communications," in *IEEE Antennas Propagat. Symp. Dig.*, Blacksburg, VA, June 1985, pp. 797–800.
[10] M. Hamer and M. Butcher, "Experimental vehicular angle-diversity antenna using mutual coupling," in *Proc. Antennas Propagat. Soc. Int. Symp.*, Chicago, IL, July 1992, vol. 2, pp. 1089–1091.
[11] R. G. Vaughan and N. L. Scott, "Antennas for FPLMTS," in *Proc. 4th Int. Symp. Personal, Indoor, Mobile Radio Commun.*, Yokohama, Sept. 1993, pp. 562–566.
[12] ——, "Evaluation of antenna configurations for reduced power absorption in the head," *IEEE Trans. Veh. Technol.*, to be published.
[13] G. F. Pedersen and J. Bach Andersen, "Integrated antennas for handheld terminals with low absorption," in *Proc. 44th IEEE Veh. Technol. Soc. Conf.*, Stockholm, Sweden, June 1994, pp. 1537–1541.
[14] R. G. Vaughan, "Two port higher mode circular microstrip antennas," *IEEE Trans. Antennas Propagat.*, vol. 36, pp. 1365–1374, Oct. 1988.
[15] O. Nørklit, P. C. F. Eggers, and J. Bach Andersen, "Jitter diversity in multipath environments," in *Proc. IEEE Veh. Technol. Soc. Conf.*, Chicago, IL, 1995, vol. 2, pp. 853–857.

Rodney Vaughan (M'84–SM'89), for a photograph and biography, see p. 990 of the July 1998 issue of this Transactions.